UCRL-TR-229835

LAWRENCE
LIVERMORE
NATIONAL
LABORATORY

Acoustic Characterization of Mesoscale Objects

D. Chinn, R. Huber, D. Chambers, G. Cole, O. Balogun, J. Spicer, T. Murray

April 10, 2007

Disclaimer

This document was prepared as an account of work sponsored by an agency of the United States Government. Neither the United States Government nor the University of California nor any of their employees, makes any warranty, express or implied, or assumes any legal liability or responsibility for the accuracy, completeness, or usefulness of any information, apparatus, product, or process disclosed, or represents that its use would not infringe privately owned rights. Reference herein to any specific commercial product, process, or service by trade name, trademark, manufacturer, or otherwise, does not necessarily constitute or imply its endorsement, recommendation, or favoring by the United States Government or the University of California. The views and opinions of authors expressed herein do not necessarily state or reflect those of the United States Government or the University of California, and shall not be used for advertising or product endorsement purposes.

Auspices Statement

This work was performed under the auspices of the U. S. Department of Energy (DOE) by the University of California, Lawrence Livermore National Laboratory (LLNL) under Contract No. W-7405-Eng-48. The project 04-ERD-013 was funded by the Laboratory Directed Research and Development Program at LLNL.

FY06 LDRD Final Report
Acoustic characterization of mesoscale objects
LDRD Project Tracking Code: 04-ERD-013
Diane Chinn, Principal Investigator

Abstract

This report describes the science and engineering performed to provide state-of-the-art acoustic capabilities for nondestructively characterizing mesoscale (millimeter-sized) objects—allowing micrometer resolution over the objects' entire volume. Materials and structures used in mesoscale objects necessitate the use of 1) GHz acoustic frequencies and 2) non-contacting laser generation and detection of acoustic waves. This effort demonstrated that acoustic methods at gigahertz frequencies have the necessary penetration depth and spatial resolution to effectively detect density discontinuities, gaps, and delaminations. A prototype laser-based ultrasonic system was designed and built. The system uses a micro-chip laser for excitation of broadband ultrasonic waves with frequency components reaching 1.0 GHz, and a path-stabilized Michelson interferometer for detection. The proof-of-concept for mesoscale characterization is demonstrated by imaging a micro-fabricated etched pattern in a 70 μm thick silicon wafer.

Introduction

Mesoscience is an emerging area of science and engineering that focuses on the study of materials with dimensions, features and structures that range from a few millimeters down to a few micrometers. Mesoscale objects typically have embedded features that require resolutions on the order of a few micrometers. Mesoscale nondestructive characterization (NDC) technologies are required that can, first, penetrate into or through a few millimeters of diverse materials and, second, provide spatial resolutions of about a micrometer over a millimeter field-of-view to cover the size of the mesoscale object.

There are a variety of established and well-known techniques to characterize surfaces, but they neither see inside nor image through mesoscale objects. For example, techniques such as electron and atomic-force microscopy can evaluate an object's surface and near-surface to very high spatial resolutions (less than a nanometer), however they cannot penetrate or "see-inside" mesoscale objects.

In the past, nondestructive techniques for mesoscale characterization have not been researched because mesoscale manufacturing capabilities have only recently become available. Understandably, characterization techniques usually develop in response to manufacturing capabilities. LLNL's FY05 acquisition of state-of-the-art 2D and 3D Xradia x-ray microscopes has enabled the first nondestructive characterization of mesoscale objects at LLNL. This new capability allows engineers to obtain an image of as-assembled internal components in mesoscale objects.

While x-ray imaging is very successful at characterizing internal structures of assembled spherical and cylindrical objects, the technique is less successful at characterizing planar objects with high aspect ratios. Acoustic testing is a technique that complements x-ray characterization. Ideally suited to planar objects, acoustic testing offers excellent characterization of interfaces where x-ray imaging falls short. An acoustic technique is attractive because it offers high sensitivity to features such as thickness and interface quality that are important to many mesoscale objects.

Of the different mesoscale characterization challenges at LLNL, the targets prepared for NIF are the most relevant. Today, we perform visual and dimensional inspection of machined components and subassemblies. The Xradia systems have brought mesoscale nondestructive characterization capability to LLNL however x-ray imaging alone is insufficient for full characterization of all target assemblies. Gigahertz frequency ultrasound for the characterization of mesoscale objects fills capability gaps left by the x-ray microscope and adds an additional, complementary characterization technique.

This research achieves micrometer resolution characterization by extending the state of acoustic testing to GHz frequencies. Materials and the geometry of components used in most LLNL mesoscale objects necessitate the use of a non-contacting technique at frequencies from 100 MHz to 10 GHz. This frequency range is required to acoustically characterize features from 5 to 0.5 μm in size. In order to be applicable to mesoscale objects, the GHz acoustic waves must propagate sufficient distances into materials of interest – for LLNL applications, mesoscale structures are on the order of 25 - 200 μm thick. In addition, this work enables new research on acoustic wave generation, scattering mechanisms and interface characterization in the GHz regime for a variety of materials.

Background

State of acoustic testing

Acoustic characterization has been in use for decades to evaluate components and materials. Most material characterization takes place in the ultrasonic frequency range (> 20 kHz) and is commonly referred to as ultrasonic testing (UT). The current state of the three common UT methods; contact, immersion and laser UT, are depicted in Fig. 1 in frequency-resolution space. Each method uses a different technique for generating and detecting acoustic waves. Contact UT uses a piezoelectric transducer in contact with the part, immersion UT uses fluid to couple a focused piezoelectric transducer to the part and laser UT uses a pulsed laser to generate and a laser interferometer to detect acoustic waves. For acoustic waves, the frequency of wave propagation is related to the wavelength by the relation

$$\lambda = \frac{c}{f} \tag{1}$$

where λ is the wavelength, c is the wave speed in the medium and f is the frequency. [Krautkramer, 1990] As a wave-based phenomenon, the spatial resolution of acoustic wave propagation, SR, is theoretically limited to the half-wavelength diffraction limit

$$SR = \frac{\lambda}{2} \tag{2}$$

According to eqns (1) and (2), obtaining a spatial resolution of 1 μm in LLNL materials of interest requires frequencies in the range of 0.5 – 10 GHz. Immersion UT capabilities currently exist to approximately 2 GHz. However, immersion UT is not suitable for mesoscale manufactured materials because (1) mesoscale objects generally cannot tolerate immersion testing (2) GHz immersion UT is physically limited to 2 GHz because of dielectric breakdown of the piezoelectric transducer used and (3) used as a surface technique, GHz immersion UT uses a highly focused transducer that penetrates less than 15 μm into materials.

Non-contact gigahertz ultrasound (GHz UT) is a solution to acoustic mesoscale characterization. Recent advances in short-pulse lasers along with current LLNL work on acoustic modeling allow this gap in acoustic characterization capabilities to be researched at this time. Commercial laser-based acoustic imaging systems are available at two discrete frequency ranges: 0.5–25 MHz, called laser UT[1], and 0.1–1 THz, or femtosecond-laser UT.[2] Laser UT has insufficient spatial resolution (~200 μm at best) for mesoscale applications. Femtosecond-laser UT is routinely used

[1] See 'LUIS–laser ultrasound inspection system' developed by Ultraoptec, Québec, Canada; www.ultraoptec.com.
[2] See '*Meta*PULSE' developed by Rudolph Technologies, Flanders, NJ, www.rudolphtech.com/reports/tech_meta_pulse.html.

in the semiconductor industry for the mechanical characterization of thin films [13]. Other unique applications of this technique include, the probing of defects in ion implanted semiconductors [14], and the mapping of micron scale sub-surface copper interconnects [15]. At present, the penetration depth of this technique is limited to about 10 μm due to the high attenuation of acoustic waves in the hundreds of GHz range at room temperature, in solid materials. The penetration depth of femtosecond laser UT is inadequate for mesoscale characterization.

Current Capabilities

Current capabilities of MHz acoustic immersion testing are illustrated in Fig. 2. A 4.3% brominated polystyrene disk, 3 mm OD, 0.5 mm thick, is glued on half of the disk to a glass plate as sketched in Fig. 2a. The disk is sealed around its edges with glue. The gap between the disk and the plate is 220 μm. Fig. 2b shows a magnified photo of the disk. A back surface image of the disk, shown in Fig. 2c, is collected by raster scanning a 50 MHz focused transducer over the disk and recording the maximum amplitude reflected from the back surface of the disk. These amplitudes are color-mapped according to the scale shown in Fig. 2c. The amplitude of the acoustic wave reflected from the back surface of the disk is an indicator of the interface conditions at the back surface. A high amplitude reflection occurs when there is an air interface or no bond at the back surface. At an air interface where there is no glue, all incident acoustic energy is reflected back from the disk/air interface. Areas with glue bonded to the disk give lower amplitude reflected acoustic waves because some energy is transmitted into the glue. Distinct areas within the glue area can be seen in the image. Low reflectivity (in red and black), indicating a good bond results when most of the acoustic energy is transmitted through the disk/glue interface. Medium reflectivity (in yellow and green) results when acoustic energy is both reflected and transmitted at the interface. This condition is deemed a "bad bond" and can result from a variety of conditions at the interface including impartial or incomplete bond or microporosity in the glue.

The spatial resolution of a focused 50 MHz transducer is approximately 48 μm in brominated polystyrene. Mesoscale characterization requires 1 μm spatial resolution, a resolution that can only be achieved for 4.3% brominated polystyrene with a frequency of 2.4 GHz.

Challenges

At the start of this project, the biggest unknown for acoustic characterization of mesoscale objects was the propagation distance of GHz waves in materials. Propagation distance is determined by attenuation of the acoustic wave and depends upon the material microstructure relative to the wavelength. Because the only previous work on GHz waves pertains to surface or near-surface inspection [Prasad, 2001] or thin film characterization [Rabe, 1996], bulk attenuation parameters at GHz frequencies do not exist in the literature.

Attenuation relationships for both polycrystalline and amorphous target materials are required for two reasons. First, sufficient propagation distance is a pivotal requirement in the use of acoustics for mesoscale characterization. Second, establishment of the attenuation, α, is required to model wave propagation at GHz frequencies. For polycrystalline materials, attenuation is a function of mean grain size, D, frequency, f, and wavelength, λ. Two types of scattering govern wave propagation, Rayleigh and stochastic scattering [Stanke, 1984 and Papadakis, 1965]:

Rayleigh scattering $\lambda >> D \quad \alpha_{PR} = T_R D f^4$, and

Stochastic scattering $\lambda \approx D \quad \alpha_{PS} = T_S D f^2$,

where T_R and T_S are empirical constants for Rayleigh and stochastic scattering, respectively.

High attenuation values in the stochastic scattering regime present the biggest challenge in characterizing micrometer-sized target features in millimeter-sized objects and subassemblies.

Amorphous material attenuation, α_A, can be described in the general case by the equation

$$\alpha_A = (1/l) \ln (p_0/p)$$

where l is the distance of propagation and p_0 and p are the amplitudes at the beginning and end of the section of length l, respectively. [Krautkramer, 1990] Acoustic properties for some aerogels, the amorphous materials used in a few target components, have been characterized at frequencies of less than 5 MHz [Gross, 1992]. Our literature search has revealed that attenuation mechanisms have not been explored for aerogels. Once a tool is available for studying GHz wave propagation, considerable research can be performed on scattering mechanisms in aerogel and other materials.

The other significant challenge to this research is to obtain mesoscale propagation distances with GHz laser UT while remaining thermoelastic. Laser generation of acoustic waves uses a short-pulse laser to heat a small area on the surface of an object (see Fig. 3a). The sudden heating and expansion of the surface creates longitudinal (P), shear (S) and surface (R) ultrasonic waves in the object. High energy flux of the generation laser generates strong longitudinal waves but can also ablate the surface. Lower energy flux produces strong shear wave components with non-ablative thermoelastic deformation of the surface. Longitudinal waves normal to the surface are more efficiently generated by lasers because the normal displacement component resulting from laser heating is the same as the normal particle motion of the wave. [Scruby, 1990] The tradeoff between propagation distance and ablative or thermoelastic wave generation must be balanced for

mesoscale objects. Some applications, e.g. rough-machined parts or parts that have surface roughness greater than the laser spot size, can tolerate ablative wave generation. Other applications, e.g. finished parts, cannot tolerate any surface damage and require thermoelastic wave generation.

Research Activities

Viability studies

Initial studies assessed the viability of mesoscale ultrasound by measuring propagation distances in materials of interest. Material attenuation coefficients, the parameter by which propagation distance can be modeled, were measured using GHz immersion UT at ORNL's High Temperature Materials Laboratory and sub-GHz laser UT at Boston University. The commercial GHz immersion UT system at ORNL could not propagate waves through most of the samples because the system uses a highly focused lens to generate GHz frequencies. Wave propagation in samples thicker than 25 μm could not be detected because of divergence of the wavefront.

The laser UT system at Boston University (BU) gave very encouraging results. Attenuation measurements with this system use the test configuration sketched in Fig. 3a. The BU system has a central frequency of 0.8 GHz. Typical signals from this configuration are shown in Figs. 3b and 3c.

Fig. 3a shows pulsed laser generation and interferometric detection of acoustic waves. The laser pulse has a wavelength 1064 nm, 1.1 ns FWHM pulse length, 4 μm spot and 0.15 μJ energy. Longitudinal (P), shear (S) and surface (R) waves are generated in the film. The longitudinal and shear waves are detected epicentrally on the opposite side of the film with a laser interferometer. The interferometer uses a CW 532 nm wavelength and has a 600 nm spot. Typical ablative and thermoelastic signals for 100 μm thick aluminum film are shown in Fig. 3b and 3c. Each peak in the signal represents an arrival of an acoustic wave at the epicentral location. In Fig. 3b, the first arrival is the longitudinal wave (P1). The next arrivals are the shear (S1) and the reflected longitudinal (P3) waves. The P3 wave is the P1 wave that has reflected off the detection surface, traveled back through the object, reflected off the generation surface, traveled back through the object and arrived back at the detection surface. Through reflected propagation, the ablative source generates a wave that travels 11 times (P11) through the thickness for a propagation distance of 1100 μm. The thermoelastically generated wave propagates 700 μm.

A table of propagation distances for materials tested is shown in Table 1.

Material	Thermoelastic propagation dist. [μm]	Ablative propagation dist. [μm]	Attenuation @0.8 GHz [dB/mm]
Aluminum	700	1100	49.9
Copper	225	525	77.8

Vanadium	225	825	52.3
Gold	200	250	58.6
Tantalum	100	200	69.6
Polystyrene	350	-	68.7
Polycarbonate	525	-	40.1
Polyamide	150	-	60.5

Table 1. Propagation distances measured for metals and polymers in ablative and thermoelastic modes can be used to calculate attenuation coefficients. Ablative wave generation was not possible in polymers.

Attenuation coefficients and propagation distances for the metals and polymers tested are shown in Table 1. In the metal/polymer sample set we used, propagation distances ranged from 100 – 700 μm for thermoelastic wave generation and from 200 – 1100 μm for ablative wave generation. From these measurements, we can conclude that mesoscale objects with thicknesses of 25 - 200 μm can be interrogated with thermoelastic or ablative wave generation. The propagation distances achieved with the BU system indicate that GHz laser UT is a viable technique for mesoscale objects.

Modeling studies

An accurate model of GHz laser UT guides the development of the system, contributes to the understanding of GHz scattering mechanisms in materials and enables simulation of characterization techniques. Attenuation coefficients derived from the viability studies are used in the model of GHz acoustic wave propagation. Our initial model uses a Gaussian distribution to simulate the laser-interaction with the surface. Acoustic wave propagation is simulated with E3D, a 2- or 3-dimensional finite-difference acoustoelastic wave modeling code developed at LLNL. [Larsen, 1998] A comparison of experimental and modeled data from 100 μm thick aluminum film is shown in Fig. 4. Attenuation and velocity of the longitudinal waves in the modeled data correlate very well with the ablative signal. Shear wave amplitudes do not correlate well because only normal components are shown for the modeled data. In acoustic characterization, the first longitudinal arrival is predominantly used for imaging.

A prototype GHz laser UT system based on the BU system was designed and assembled at LLNL. A schematic of the system is shown in Fig. 5.

Proof of concept

As a proof of concept, the GHz laser UT system was used to image a micro-fabricated sub-surface pattern etched 3 μm into a (100) silicon wafer of thickness 70 μm. The generation and detection lasers were aligned on epicenter on the un-patterned surface of the silicon wafer, and several bulk ultrasonic echoes reflecting from the patterned surface

of the wafer were detected. The bandwidth of the generated and detected ultrasound is about 1 GHz, and ultrasonic echoes with propagation distances as large as 400 μm, were detected with sufficient signal-to-noise ratio. The lateral spatial resolution of the laser acoustic microscopy system at the imaging depth is 36 μm, which is approximately $4\lambda_c$, where λ_c is the wavelength of the laser generated ultrasonic wave pulse at the limiting frequency. The lateral spatial resolution of the system is an improvement on the previous LBU work on sub-surface acoustic microscopy [15], where the best lateral spatial resolution obtained is about $70\lambda_c$, and the image depth is 6 μm.

Experimental setup

In the prototype setup n Fig. 5, a neodymium yittrium aluminum garnet (Nd:YAG) microchip laser is used for ultrasonic wave generation. The microchip laser has a peak pulse energy of 50 μJ, a pulse width of 900 ps, a repetition rate of 50 KHz, and its wavelength is 1064 nm. The generation laser is collimated and delivered to a gimbal scanning mirror. The reflected beam from the gimbal mirror passes through a set of relay lenses, a dichroic mirror, and is focused by a 20x long distance microscope objective on the sample surface to a minimum circular spot of diameter D ~ 3 μm, at the full width at half maximum (FWHM) intensity level. The separation distances between the gimbal mirror, the relay lenses, and the microscope objective is chosen such that these optics are configured as a 4*f* imaging system. The 4*f* imaging system is used to scan the generation laser spot on the sample surface, by changing the entry angle of the laser into the microscope objective. The normal displacement associated with the generated ultrasound is detected using a path stabilized Michelson interferometer. The interferometer uses a frequency doubled Nd:YAG detection laser with a wavelength of 532 nm. The detection laser is delivered into the experimental setup through a single mode optical fiber, is collimated, and directed to a beam splitter which splits the light into signal and reference beams. The signal beam is directed to the sample surface through the microscope objective, and redirected on reflection from the sample surface to a high speed photodetector with a rise time of 1 ns. The circular diameter of the signal beam on the sample surface is 1.2 μm at the FWHM. The reference beam is delivered to a reference mirror, which redirects the beam to the photodetector, where it interferes with the signal beam producing an intensity modulated signal that is related to the absolute displacement

of the sample surface. The interferometer is stabilized at the point of maximum displacement sensitivity through active adjustment to the optical path length difference between the reference and signal beams. This is achieved by electronically dithering the reference mirror which is mounted on a piezoelectric actuator. The output signal from the photodetector is digitized in a LeCroy oscilloscope at the rate of 10 GS/s, and sent to a computer for data processing. The sample is supported on a three axis translation stage, and a Labview computer program is used to control the translation stages, as well as to trigger the oscilloscope for data acquisition.

SAMPLE FABRICATION

Figure 6 shows a schematic of the test sample. The sample consists of a 70 μm thick (100) single-crystal silicon wafer with one face etched to produce a patterned surface using standard photolithography techniques. Due to the long absorption depth of the generation laser in silicon, which limits the bandwidth of the generated ultrasound, a 207 nm thick aluminum film was deposited on the un-etched side of the wafer. The optical skin depth of the generation laser in the aluminum film is less than 20 nm, allowing for the optimal generation of broad bandwidth ultrasound in the silicon sample. The photomask used to generate the etched topography was originally designed for the fabrication of micromechanically-tunable vertical-cavity optical amplifiers [17]. This mask was chosen for its appropriate dimensions as well as the variety of geometries present, including orthogonal and curved features. The silicon wafer was initially cleaved to obtain small chips of top dimensions 1 cm X 1 cm. The cleaved chips were patterned using a deep reactive ion etch system with a standard cyclic process (SF_6 as the etchant, alternating with C_4F_8 for passivation) and protected with a photoresist mask. To improve thermal transfer during etching, the silicon chips were mounted on a carrier wafer using the photoresist. The exposed silicon surface was etched for 2.5 minutes, resulting in a feature height of approximately 3.5 μm. Following the silicon etch, the chips were removed from the carrier wafer and the masking resist was stripped using a combination of organic solvents and oxygen plasma ashing. After a thorough cleaning, an aluminum film was deposited on the unpatterned surface by electron beam evaporation.

MEASUREMENT AND SIGNAL ANALYSIS APPROACH

The generation and detection lasers were aligned on the sample surface coated with the aluminum film. The spot size of the generation laser on the sample surface was expanded to a diameter of about 30 μm, by adjusting the position of the relay lenses, which defocuses the light. This was done in order to avoid ablating the sample, as well as to maximize the total laser energy deposited in the sample. Figure 7a shows a time trace of the normal displacement measured at a point on the sample surface. The waveform was averaged 700 times in the oscilloscope to minimize the incoherent noise in the data. The waveform shows a rapid thermal expansion following the incidence of the laser pulse on the sample surface, and it decays slowly with time. Several transient arrivals corresponding to acoustic wave reflections from the bottom surface of the sample, and a low frequency ringing signal that lasts for several nanoseconds, are also present in the waveform. Identifying the acoustic wave transients can be challenging for two reasons. First, the amplitude of the acoustic waves is small. The second reason is that the wave propagation direction corresponds to the <110> direction, which supports several acoustic modes including the quasi-longitudinal, pure shear, and quasi-shear, and mode converted shear/longitudinal waves, which arrive close to each other. In order to identify these acoustic wave reflections, the thermal expansion signal seen in Fig. 7a was removed by bandpass filtering the measured signal between 300 MHz and 1.2 GHz. The filtered waveform obtained is shown in Fig. 7b. The longitudinal wave reflections labeled as P2, P4 & P6 in the figure are clearly identified in the filtered waveform. The P2 reflection has a pulse width of about 1.2 ns, and a cut-off frequency of approximately 1.0 GHz. The time difference between successive peaks or troughs of the longitudinal wave reflections is 14.8 ns as seen in Fig. 7b. The time difference Δt is related to the quasi-longitudinal wave velocity C_1, and the sample thickness h, by $\Delta t = 2h/C_1$. Taking $C_l = 9.13$ μm/ns along the <110> direction in silicon [2], the sample thickness is estimated to be 68 μm, which is close to the nominal value of 70 μm quoted by the manufacturers. It is also important to point out that the P6 reflection traversed a total distance of 408 μm, and its amplitude is clearly visible above the noise floor. This indicates that the laser acoustic microscopy system may be suitable for probing structural or mechanical features at mesoscopic length scales.

The longitudinal and shear wave reflections present in Fig. 7b can also be identified in the frequency domain by searching for amplitude peaks in the magnitude spectrum. These peaks occur at fundamental frequencies corresponding to the ratio of the time period of the echoes, or at the harmonics of the fundamental frequency. The quasi-longitudinal wave, for instance, has a fundamental thickness resonance at 67.6 MHz; this frequency corresponds to the reciprocal of the time period of the quasi-longitudinal wave echoes seen in Fig. 7b. Figure 7c shows the magnitude spectrum obtained by taking the Fourier transform of Fig. 7b. An amplitude peak is identified close to the fundamental thickness resonance of the quasi-longitudinal wave, in addition to harmonics of the quasi–longitudinal, quasi-shear, and pure shear thickness resonance modes. The prominent amplitude peak at 410 MHz corresponds to a harmonic of the quasi-shear thickness resonance; its peak amplitude is large compared to the background noise. The width of the resonance is narrow, indicating that the resonance frequency is sensitive to changes in the mechanical and structural properties of the sample. Note that the amplitudes of the resonance peaks below 300 MHz in Fig. 7c are in fact larger than the 410 MHz peak, and they appear smaller in the figure due to the 300 MHz low frequency pass-band of the filter applied to the measured waveform. Since the goal of this work is the detection of small scale defects, measurement of the 410 MHz resonance peak is more advantageous than the low frequency resonances because of its higher sensitivity.

In order to map the etched pattern below the aluminum side of the silicon sample, the arrival time t of the peak amplitude of the P2 reflection in the bandpass filtered waveform, and the resonance frequency of the quasi-shear thickness resonance close to 410 MHz, are monitored as the sample is scanned over the measurement area.

3. RESULTS AND DISCUSSION

A. SUB-SURFACE IMAGING

Figure 8a shows the C-scan image of the arrival time of the peak amplitude of the P2 reflection measured over a 400 μm X 400 μm area. In this experiment, the sample was raster scanned in 5 μm steps, and the waveform obtained at each measurement point was

analyzed as explained in section 2C. The change in arrival time of the P2 reflection seen in the C-scan reveals the etched pattern at the bottom of the sample. An SEM image of the pattern taken from the etched side of the sample is shown in Fig. 8b. The etched pattern in the C-scan and the SEM image are in good agreement. The slight tilt in the etched pattern seen in the C-scan image with respect to the SEM image, results from the fact that the sample was not aligned with respect to a common reference frame when both images were taken. The maximum change in arrival time of the P2 reflection observed in the C-scan image is about 0.8 ns, which corresponds to a thickness change of 3.6 μm. The sample thickness change, which corresponds to the height of the etched sub-surface pattern, is close to the expected value of 3.5 μm. Figure 8c shows a C-scan image of the quasi-shear thickness resonance frequency measured over the same area. The change in quasi-shear thickness resonance frequency seen in the figure reveals the sub-surface pattern, and it results from the change in sample thickness arising from the presence of the sub-surface pattern. A maximum frequency shift (Δf) of 24 MHz is seen in the image, which is related to the sample thickness change by $\Delta h = (\Delta f/f)h$, where h = 68 μm is the thickness of the un-etched silicon sample. Using the expression for Δh, the height of the etched pattern obtained from the resonance C-scan image is 4.0 μm, which is slightly greater than the value obtained from the time of flight C-scan image. The reason for the disparity in the measured height of the etched pattern is unclear. The ability to resolve the sub-surface pattern demonstrates the high sensitivity of the laser acoustic microscopy system to micrometer scale features at mesoscopic length scales. Furthermore, these measurements can be conducted using a broadband approach in which transient longitudinal or shear wave modes are generated and detected, or a narrowband approach based on the excitation of the thickness resonances.

B. LATERAL SPATIAL RESOLUTION AND EDGE EFFECTS

In order to determine the lateral spatial resolution of the experimental setup, a line scan was taken across an edge in the sub-surface pattern with a step size of 1 μm. Figure 9a & 9b shows the measured edge response obtained by measuring the peak amplitude and the corresponding arrival time of the P2 reflection. The measured data were fitted with a Gaussian and sigmoidal functions for the amplitude and time plots, and the fitted results

are shown in the vicinity of the edge in the figures. The peak amplitude of the P2 wave reflection decreases as the wave interacts with the abrupt edge as seen in Fig. 9a, producing an edge width of 36 μm, which corresponds to the FWHM of the curve fit. The broad edge width obtained can be attributed to pronounced acoustic scattering and diffraction effects that occur in the neighborhood of the edge. The lateral spatial resolution of the laser acoustic microscopy system, estimated based on an edge width of 36 μm is about $3.9\lambda_c$, where $\lambda_c = 9.13$ μm, and it is the critical acoustic wavelength of the quasi-longitudinal wave in silicon along the thickness direction, at the cut-off frequency of the wave. The lateral spatial resolution of the system is an improvement on the previous LBU work on sub-surface acoustic microscopy [15], where the best lateral spatial resolution obtained is about $70\lambda_c$, and the feature depth is 6 μm. Furthermore, the lateral spatial resolution of the system can be improved on by increasing the bandwidth of the laser generated ultrasound, which ultimately reduces λ_c. This can be achieved by using a shorter generation laser pulse.

The edge response obtained from monitoring the arrival time of the P2 reflection is shown in Fig. 9b, and it yields a smaller edge width than is seen in Fig. 9a. The width of the transition region corresponding to the step change in thickness of the sample is less than 10 μm. The transition region shows a high degree of uncertainty in the measured time, which is due to the low amplitude of the P2 reflection in this region, arising from strong acoustic scattering effects close to the edge. Assume that the physical shape of the edge can be approximated by a step function, the lateral spatial resolution of the laser acoustic microscopy system can also be estimated based on the width of the line spread function. The line spread function is shown in Fig. 9c, and it was obtained from the deconvolution of the sigmoidal fit to the measured edge response, and the step function. The FWHM of the line spread function indicates that a sub-critical wavelength lateral spatial resolution of 4 μm is obtained by measuring the arrival time of the P2 reflection. This result may appear to be anomalous at first examination. However, the super lateral spatial resolution obtained can be attributed to interference effects that occur close to the edge, resulting from the lack of sufficient temporal resolution to separate echoes from the top and bottom of the edge step. The time delay between the longitudinal wave

reflections from the top and bottom of the edge is 0.8 ns, which is less than the temporal width of the P2 reflection. Consequently, the reflected longitudinal wave pulses from the top and bottom of the edge overlap in time and interfere. This temporal interference effect proves to be advantageous in this case, because it yields a lateral spatial resolution that is better than the diffraction limited case obtained from the amplitude data.

4. CONCLUSION

In this work, a GHz laser UT system designed for the detection of micrometer scale defects in mesoscale structures was presented. The laser acoustic microscopy system is configured as a point -source point-receiver system, and it allows for the generation and detection of broadband ultrasound with frequency components close to 1 GHz. The feasibility of using the laser acoustic microscopy system for mesoscale mechanical characterization was demonstrated by mapping a micro-fabricated sub-surface pattern etched into a (100) silicon wafer with a nominal thickness of 70 μm. It was shown that the laser acoustic microscopy system is capable of generating and detecting GHz ultrasonic waves over propagation distances of at least 400 μm. The spatial resolution of the system measured at a feature depth of 68 μm is approximately $4\lambda_c$, where λ_c is the wavelength of the laser generated ultrasonic wave pulse at the limiting frequency. The lateral spatial resolution is limited by acoustic scattering and diffraction, which are pronounced at abrupt edges in a sample. Future work will be directed at improving on the lateral spatial resolution of the system, such that it approaches 1 μm over comparable object depths. This can be achieved by increasing the bandwidth of the generated ultrasound by using a shorter generation laser pulse. This work clearly demonstrates the feasibility of detecting micrometer scale internal defects in mesoscale structures using laser acoustic microscopy techniques at operational frequencies in the GHz range.

Exit Plan

This new NDC technique is intended to complement other NDC techniques at LLNL for mesoscale characterization. Follow-on work includes an Engineering Tech Base project to apply this fundamental research to LLNL applications such as interface characterization of planar EOS

targets and gas gun targets, ice thickness measurements of cryo-targets and density measurements of biological samples.

References

Albrecht, G., private conversation May 27, 2005.

Chambers, D., D. Chinn, and R. Huber (2004), "Optical mapping of the acoustic output of a focused transducer", Proceedings of the 147th Acoustical Society of America Meeting.

Gross, J., J. Fricke, and L. Hrubesh (1992), Sound propagation in SiO_2 aerogels, Lawrence Livermore National Laboratory, Livermore, CA, UCRL-219781.

Krautkramer, J., and H. Krautkramer (1990), Ultrasonic Testing of Materials (Springer-Verlag, New York, NY).

Larsen, S., and Grieger, J. (1998), "Elastic modeling initiative, Part III: 3-D computational modeling," Lawrence Livermore National Laboratory, Livermore, CA, UCRL-JC-130224.

Papadakis, E. (1965), "Revised grain-scattering formulas and tables," Journal of the Acoustical Society of America 37, p. 4.

Prasad, M. (2001), "Mapping impedance microstructures in rocks with acoustic microscopy", The Leading Edge, pp172 - 179.

Rabe, U., W. Arnold (1996), "Acoustic microscopy with resolution in the nm-range", Acoustical Imaging, 220, pp. 669 - 676.

Richardson, C., J. Spicer, R. Huber, P. Thielen, and H. Lee (2001), "High frequency laser based NDT of extreme ultraviolet lithography masks," Materials Evaluation 59 (10), pp. 1223-1226.

Stanke, F., and G. Kino (1984), "A unified theory for elastic wave propagation in polycrystalline materials," Journal of the Acoustical Society of America 75 (3), pp. 665-681.

Scruby, C. (1990), Laser Ultrasonics: techniques and applications (Adam Hilger, New York, NY).

1. G.A.D. Briggs, *An Introduction to Scanning Acoustic Microscopy*, (Oxford University Press, Oxford, UK, 1985)

2. A. Briggs, *Acoustic Microscopy*, (Clarendon Press, Oxford, UK, 1992)

3. C.B. Scruby and L.E. Drain, Laser Ultrasonics, Techniques and Applications, (Adam Hilger, N.Y., 1990)

4. S.J. Davies, C. Edwards, A.D.W. Mckie, and J.W. Wagner, J. Phys. D: Appl. Phys. ,**26**(3), 329, (1992)

5. A. Neubrand and P. Hess, J. Appl. Phys., **71**(14), 2974, (1992)

6. J.B Spicer and S.L. Wallace, J. Mater. Sci. **33,** 3899, (1998)

7. T.W. Murray, S. Krishnaswamy, and J.D. Achenbach, Appl. Phys. Lett. **74**(23), 3561, (1999)

8. J.A. Rogers, A.A. Maznev, M.J. Banet, and K.A. Nelson, Annu. Rev. Mater. Sci., **30**, 117, (2000)

9. O. Balogun and T.W. Murray, J. Appl. Phys., **100**, 034902-1, (2006)

10. C. Thomsen, H.T. Grahn, H.J. Maris, and J. Tauc, Phys. Rev. B, **34**(6), 4129, (1986)

11. A. Vertikov, M. Kuball, A.V. Nurmikko, and H.J. Maris, Appl. Phys. Lett. **69**(17), 2465, (1996)

12. B.C. Daly, N.C.R. Holme, T. Buma, C. Branciard, and T.B. Norris, Appl. Phys. Lett. **84**(25), 5180, (2004)

13. H.J. Maris, Scientific American, **278**, 64, (1997)

14. G. Tas, J.J. Loommis, H.J. Maris, A.A. Bailes III, and L.E. Seiberling, Appl. Phys. Lett. **72**(18), 2235, (1998)

15. S. Ramanathan, and D.G. Cahill, J. Mater. Res. **21**(5), 1204, (2006)

16. G.D. Cole, E.S. Bjorlin, Q. Chen, C.Y. Chan, S. Wu, C.S. Wang, N.C. McDonald, J.E. Bowers, IEEE J. Quant. Elect. **41**(3), 390, (2005)

Figures

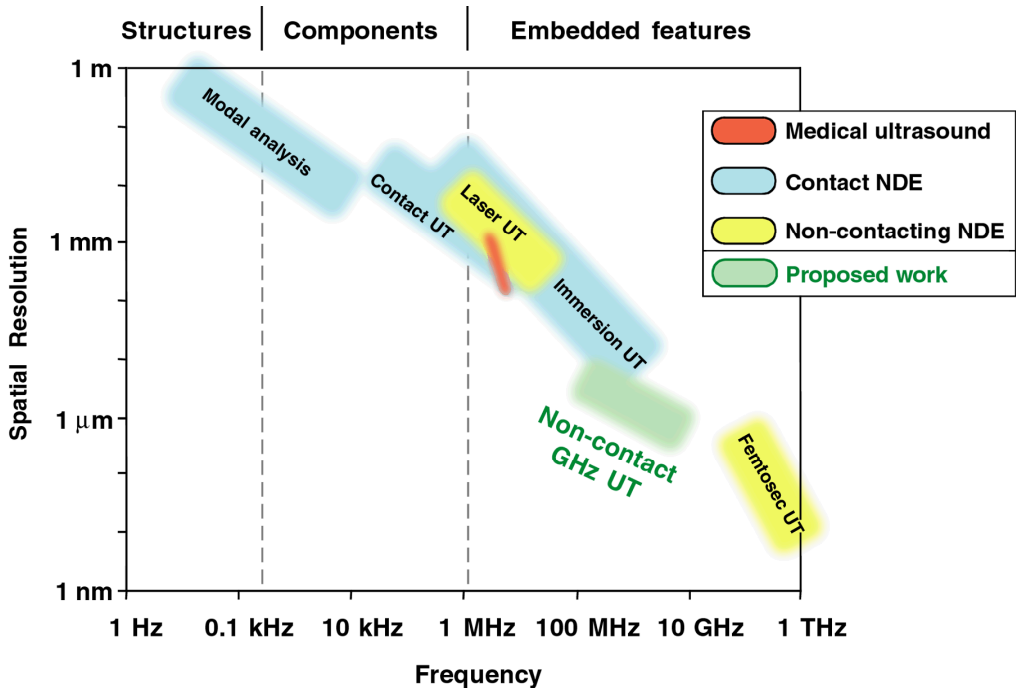

Figure 1. The chart shows two key parameters describing acoustic characterization, frequency and spatial resolution. Ranges of existing contacting (contact and medical) and non-contacting (laser) methods are shown. The range of this research (shown in green) extends to a range not covered by existing techniques.

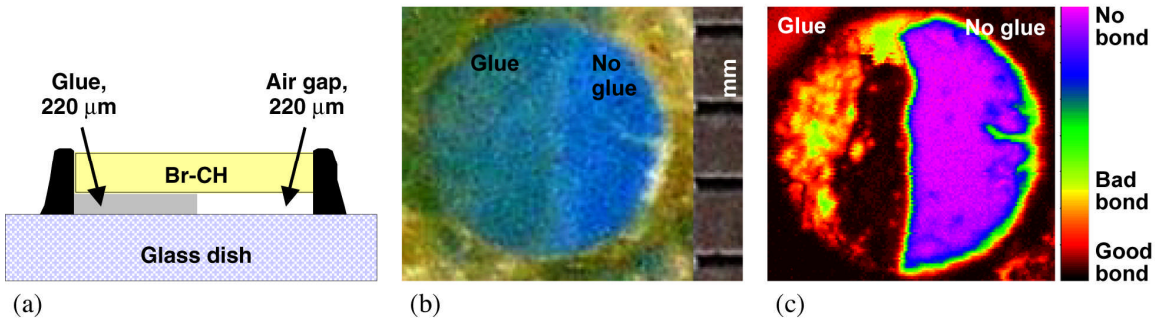

Figure 2. A 4.3% brominated polystyrene disk glued to a glass dish (sketch in a, photo in b). An ultrasonic scan (in c) shows areas of no bond, bad bond and good bond.

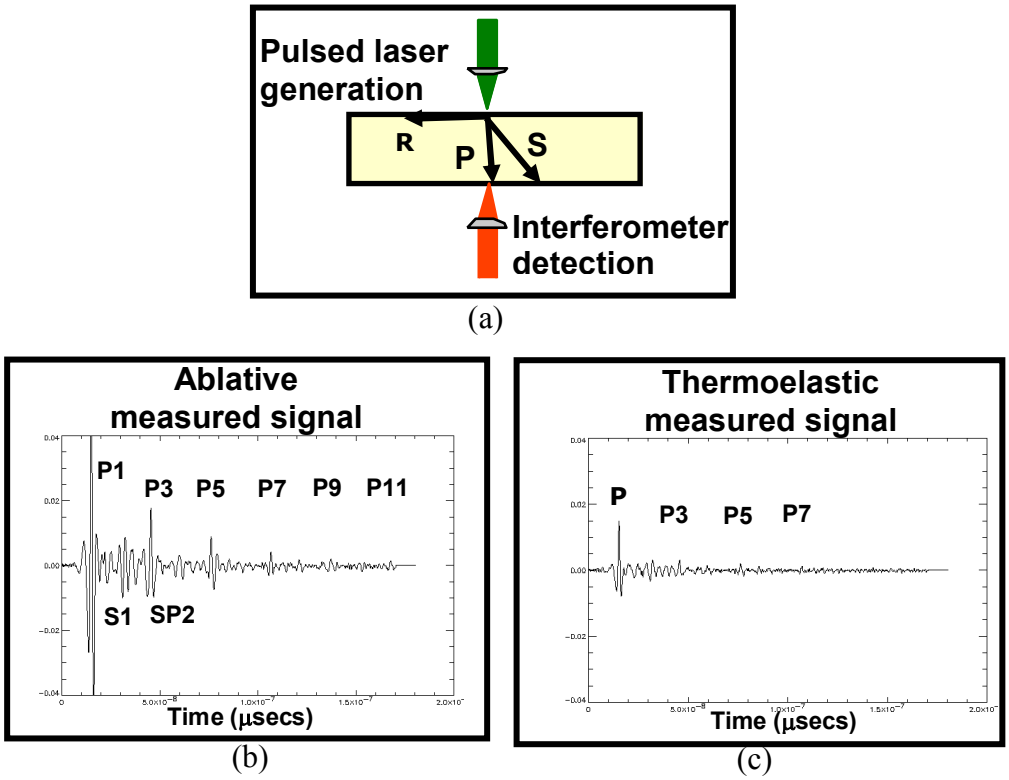

Figure 3. The test configuration is shown in (a). Data collected from a 100 μm thick aluminum film is shown in ablative mode (b) and thermoelastic mode (c).

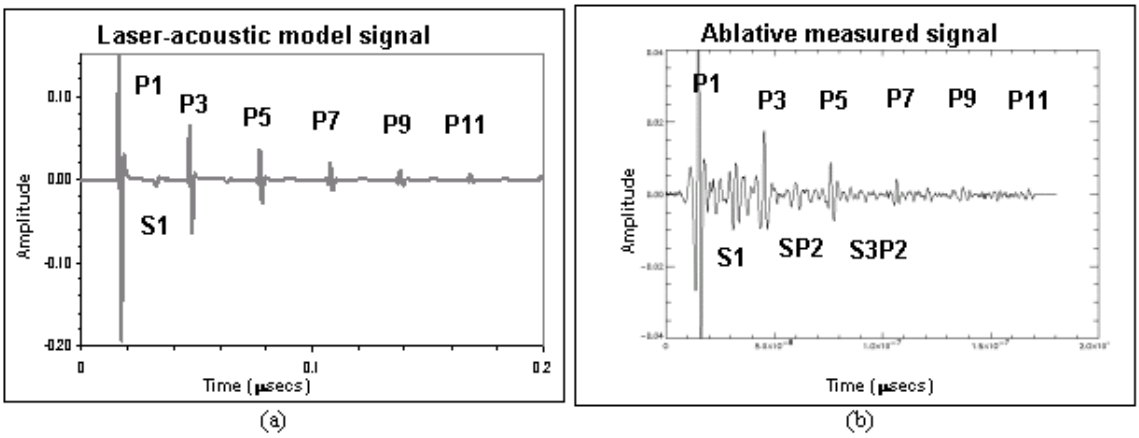

Figure 4. Modeled (a) and measured (b) signals for a 100 μm thick aluminum film show good correlation. The modeled signal only shows normal components and as such does not capture shear modes adequately.

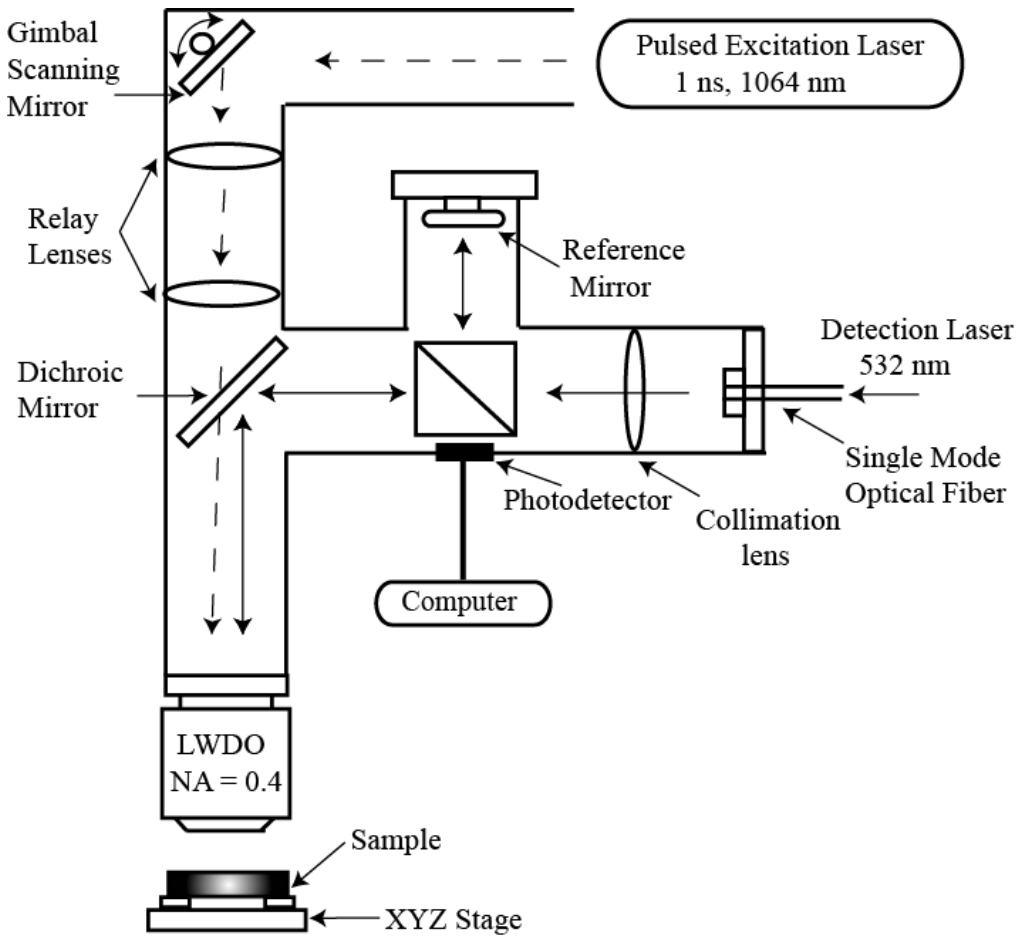

Figure 5. Major components of the GHz laser UT prototype include the pulsed excitation laser, detection laser, and the precision XYZ scanning stage. The LWDO – Long working distance microscope objective has a numerical aperture (NA) of 0.4.

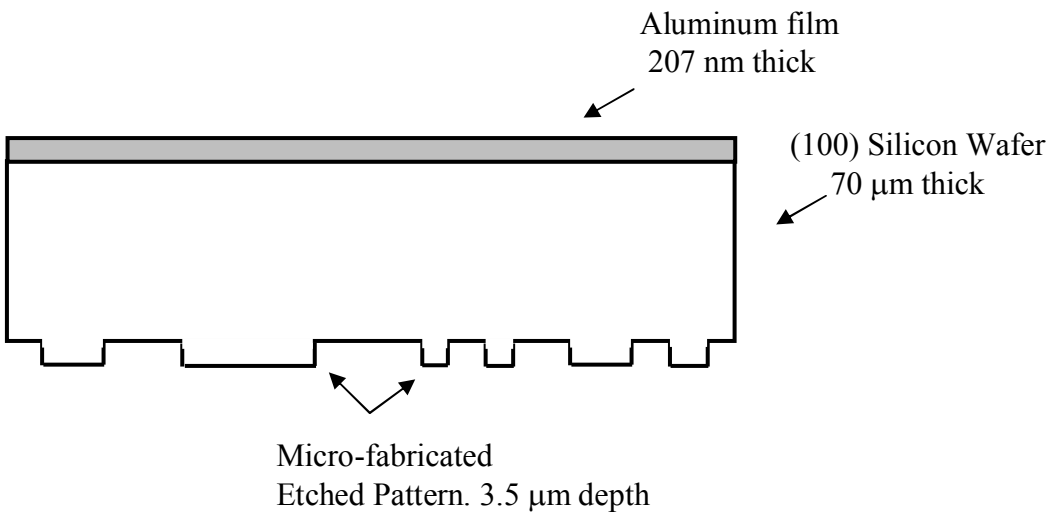

Figure 6. Geometry of the micro-fabricated silicon sample.

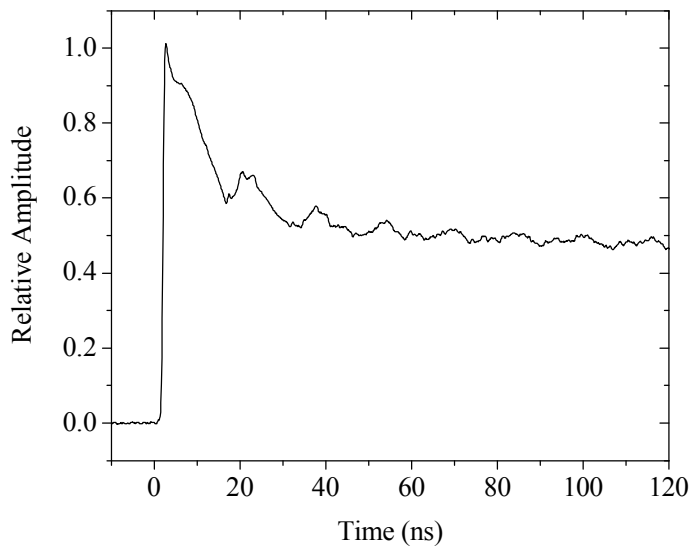

Figure 7a. Raw waveform from silicon sample.

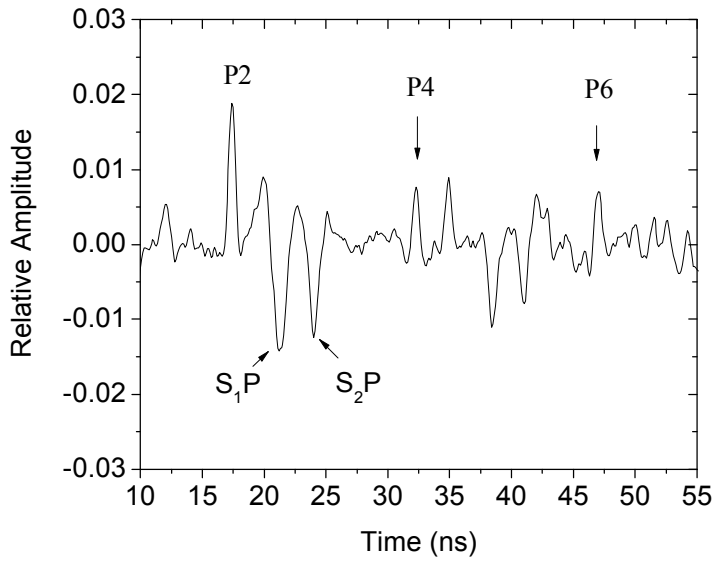

Figure 7b. Bandpass filtered waveform (300 MHz – 1.2 GHz) shows arrival of bulk waves.

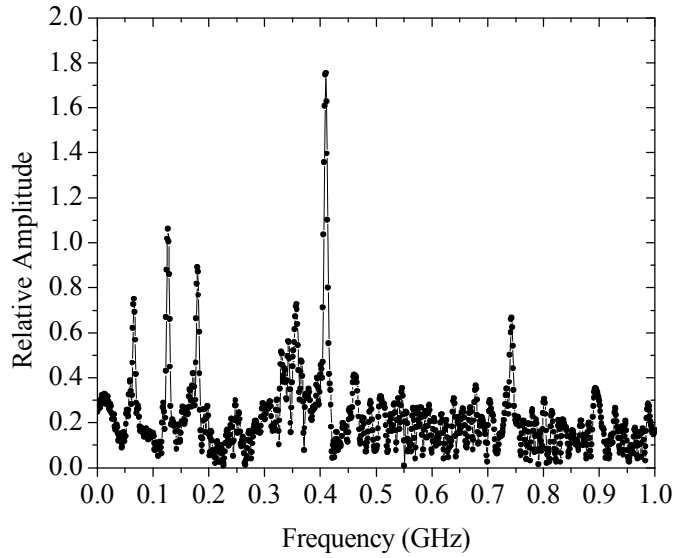

Figure 7c. Frequency spectrum of the bandpass filtered waveform shows peaks at fundamental thickness resonance modes.

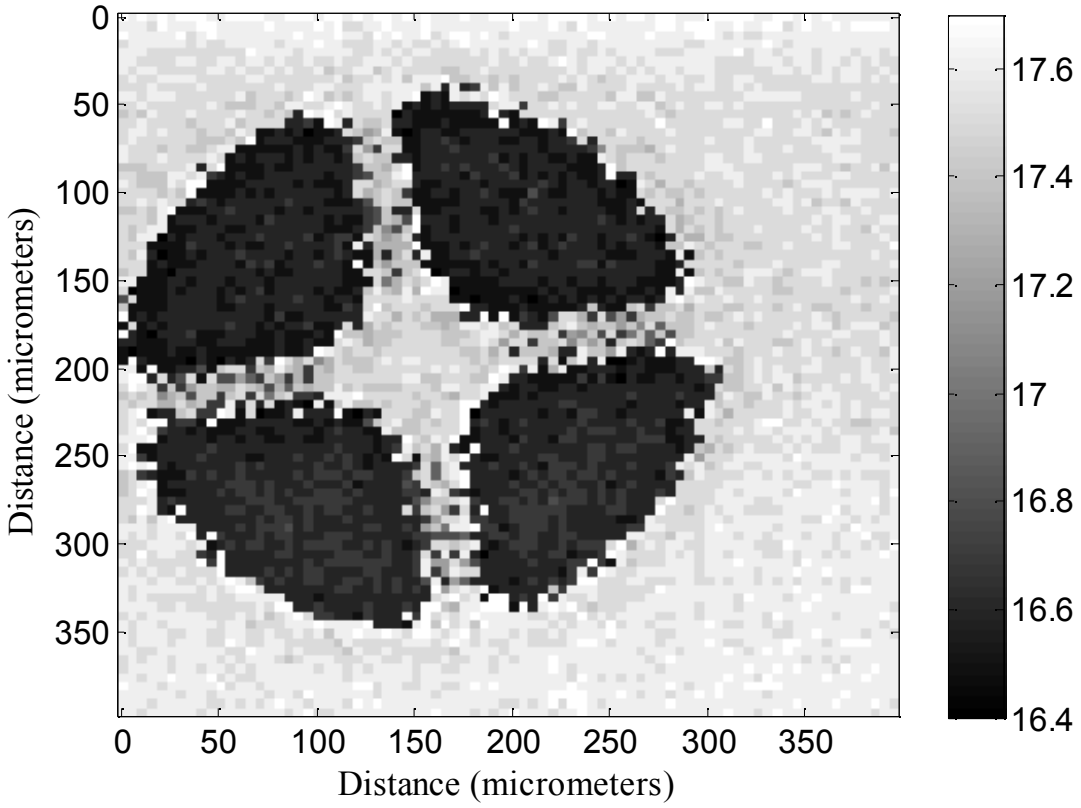

Figure 8a. A 400 μm x 400 μm C-scan image of the P2 reflection amplitude with 5 μm steps shows the etched shape in the silicon.

Figure 8b. An SEM image of the etched pattern shows good agreement with the C-scan image.

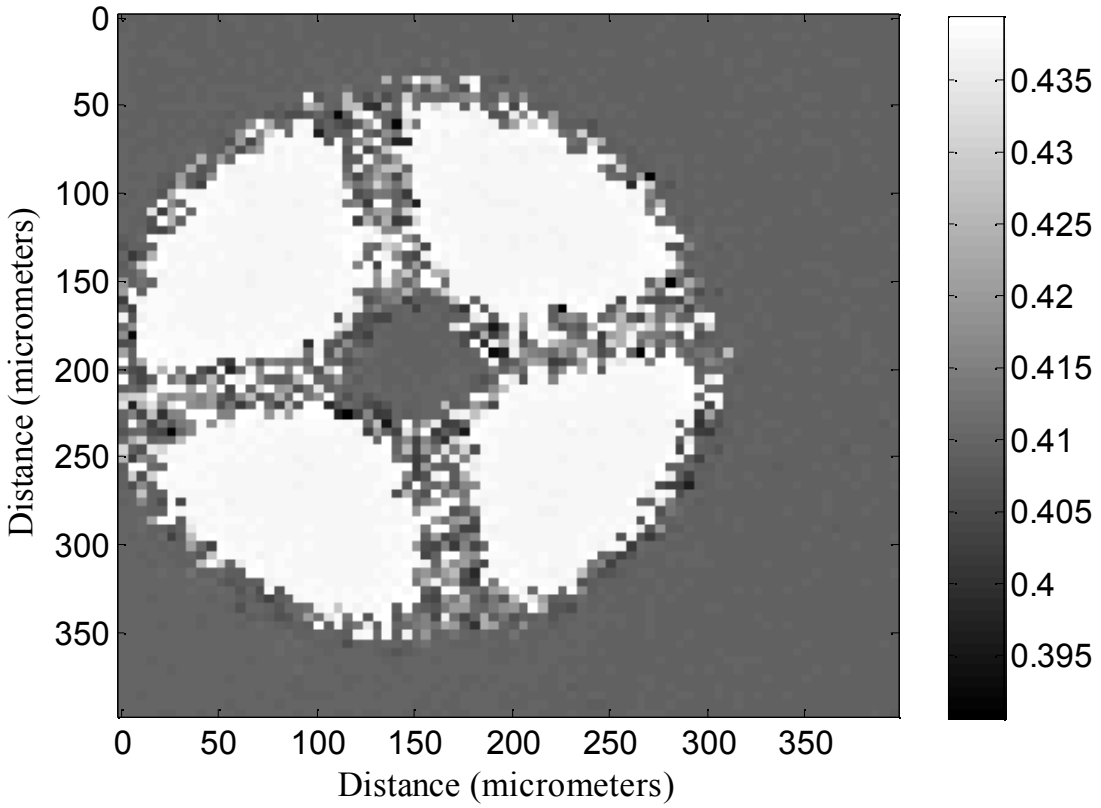

Figure 8c. A C-scan image mapping the spectral value of the quasi-shear thickness resonance peak close to 400 MHz is sensitive to thickness variations.

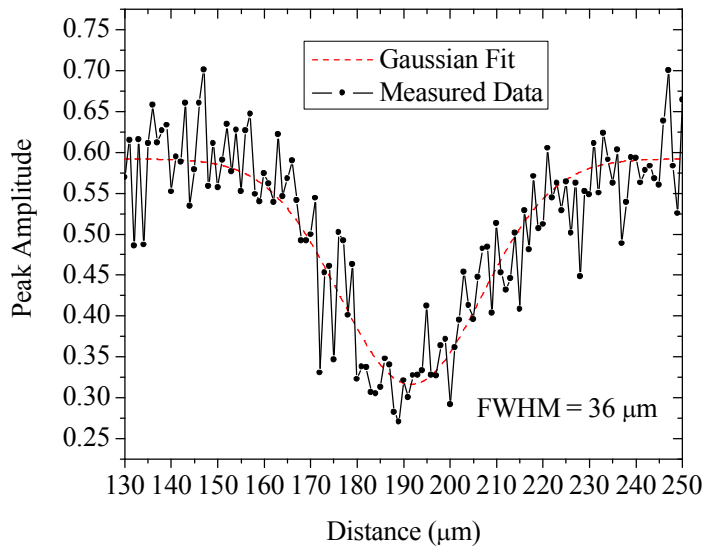

Figure 9a. A line-out across a feature edge from the P2 C-scan amplitude image in Fig. 8a shows an edge response FWHM of 36 μm.

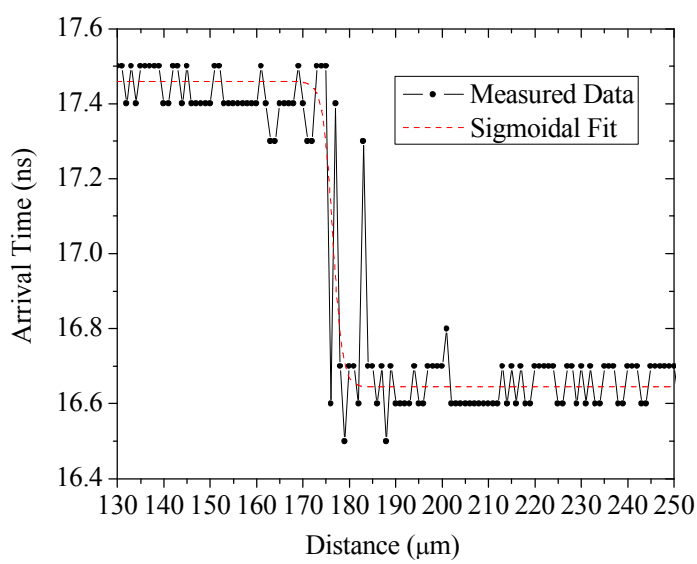

Figure 9b. A line-out across a feature edge from the time-of-flight C-scan image shows an edge response with a sigmoidal fit.

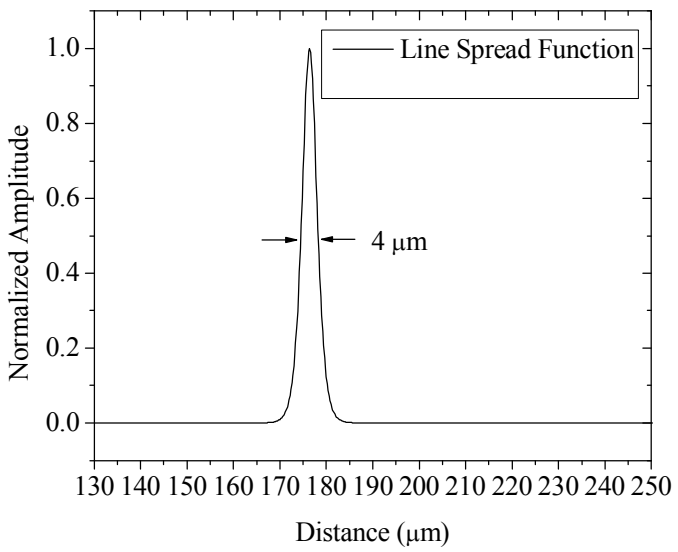

Figure 9c. The line spread function of the edge response in Fig. 9b is obtained from the deconvolution of the P2 wave arrival time sigmoidal fit with a step function.